Broadband Coherent Enhancement of Transmission and Absorption in Disordered Media

Chia Wei Hsu, Arthur Goetschy, Yaron Bromberg, A. Douglas Stone, and Hui Cao

Phys. Rev. Lett. **115**, 223901 — Published 25 November 2015

DOI: 10.1103/PhysRevLett.115.223901

Broadband Coherent Enhancement of Transmission and Absorption in Disordered Media

Chia Wei Hsu,[1] Arthur Goetschy,[2] Yaron Bromberg,[1] A. Douglas Stone,[1] and Hui Cao[1]

[1]*Department of Applied Physics, Yale University, New Haven, Connecticut 06520, USA**

[2]*ESPCI ParisTech, PSL Research University, CNRS, Institut Langevin, 1 rue Jussieu, F-75005 Paris, France*

Spatial modulation of the incident wavefront has become a powerful method to control the diffusive transport of light in disordered media; however, such interference-based control is intrinsically sensitive to frequency detuning. Here we show analytically and numerically that certain wavefronts can exhibit strongly enhanced total transmission or absorption across bandwidths that are orders of magnitude broader than the spectral correlation width of the speckles. Such broadband enhancement is possible due to long-range correlations in coherent diffusion, which cause the spectral degrees of freedom to scale as the square root of the bandwidth rather than the bandwidth itself.

One exciting development in optics in recent years is the coherent control of diffusing light in a disordered medium by shaping input wavefronts using a spatial light modulator (SLM) [1, 2]. Initially the emphasis was on using wavefront shaping (WFS) to focus light onto a wavelength-scale region (speckle) behind or within the disordered medium [3, 4], with potential applications for imaging; the optimal input wavefront in this case can be found by a simple sequential optimization of each pixel on the SLM, since each contributes to the local field at the focal spot independently. More recently there has been progress in the more challenging problem of optimizing *global* properties of the fields, such as the total transmitted power through the medium [5–7]. Motivation came from theoretical concepts first formulated in the context of mesoscopic electron transport and localization theory [8–11], where it was predicted that in a lossless diffusive medium there would always exist sample-specific "open channels" that will be transmitted almost perfectly. A closely related effect is the coherent enhancement of absorption (CEA) to near unity via WFS in a disordered medium that on average only absorbs a small fraction of the input light [12, 13]. Incomplete control of the input wavefronts reduces the possible enhancements [14, 15], but large enhancements are still observable under realistic conditions [6, 13].

The physical basis of these coherent control effects is manipulation of the multiple-scattering interference in the medium. Hence these effects would seem to be intrinsically narrowband, limiting their applications in contexts such as power delivery, communications, or energy conversion, in which larger bandwidths may be required. The expected bandwidth is limited by the frequency correlation scale, $\delta\omega$, which for transmission is the inverse of the time to diffuse across the thickness L of the medium, $\delta\omega \approx D/L^2$ ($D = lc/d$ is the diffusion constant in d dimensions, and l is the transport mean free path) [16]; for CEA, $\delta\omega \approx c/l_a$, where l_a is the ballistic absorption length [12]. For a broadband signal with bandwidth $\Delta\omega \gg \delta\omega$, a natural hypothesis is that the effective number of independent frequencies would be $M_{\text{eff}} \approx 1 + \Delta\omega/\delta\omega$, and that the maximal achievable enhancement decreases as $1/M_{\text{eff}}$. Indeed this is exactly the behavior found in experiments maximizing the focal intensity of polychromatic light on a single speckle spot using SLMs [17–20]. However we will show that this is not the case for the total transmission or absorption due to the long-range spectral correlations of coherent diffusion [21–24], which are unimportant for speckle statistics but play a major role for the global properties [16, 22, 25–28]. These correlations dramatically reduce the effective number of independent degrees of freedom, and instead of the linear scaling, we find $M_{\text{eff}} \approx \sqrt{\Delta\omega/\delta\omega}$, allowing substantial coherent control of transmission and absorption over large bandwidths. For example, for a lossless diffusive sample with average 2% transmission, the total transmission can be enhanced 10 times across bandwidth $\Delta\omega \approx 60\delta\omega$; similarly for a thick diffusive sample with average 3% absorption, the total absorption can be enhanced 10 times across $\Delta\omega \approx 60\delta\omega$.

We begin by defining a broadband flux matrix, based on the monochromatic transmission matrix $t(\omega)$ that relates the incident field $|\psi_{\text{in}}\rangle$ to the transmitted field $|\psi_{\text{t}}\rangle = t|\psi_{\text{in}}\rangle$; the field vectors are written in the basis of N input and output modes carrying unit flux, and we assume $N \gg 1$. The monochromatic transmitted flux $\langle\psi_{\text{t}}|\psi_{\text{t}}\rangle$ is the expectation value $\langle\psi_{\text{in}}|t^\dagger(\omega)t(\omega)|\psi_{\text{in}}\rangle$ of the Hermitian matrix $t^\dagger t$; it follows that the most open channel for monochromatic light corresponds to the largest eigenvalue of $t^\dagger t$ [8–11, 29–34]. For polychromatic light, the role of $t^\dagger t$ is replaced by

$$A = \int d\omega I(\omega) t^\dagger(\omega) t(\omega), \tag{1}$$

where $I(\omega)$ is the power spectrum of the incident light normalized to $\int d\omega I(\omega) = 1$. When the transmitted flux is measured with a sufficiently-long integration time, beating between different frequencies averages away, and the total transmission for incident light with spectrum $I(\omega)$ and wavefront $|\psi_{\text{in}}\rangle$ is simply $\langle\psi_{\text{in}}|A|\psi_{\text{in}}\rangle$. Since A is still Hermitian, the optimal wavefront is again given by

the eigenvector with the largest eigenvalue. A broadband reflection flux matrix can be defined similarly, with $r^\dagger r$ replacing $t^\dagger t$. Note that a monochromatic open channel is generally not an eigenvector of A, so it will not provide the optimal broadband transmission. As we shall see later in Fig. 2(b), the optimal wavefront has its transmission enhanced rather uniformly across the target bandwidth, so optimizations aiming for spectral uniformity (such as maximin) will yield similar results.

In the diffusive regime ($\lambda \ll l \ll L$, where λ is wavelength), each matrix $t^\dagger(\omega)t(\omega)$ has a bimodal eigenvalue density $p_{t^\dagger t}(T) = \bar{T}/(2T\sqrt{1-T})$ where $\bar{T}$ is the average transmission [8–11]; the effect of absorption is considered in Ref. [35]. The distribution has support up to $T = 1$, meaning monochromatic open channels always exist in the diffusive regime. Since the transmission matrices at different frequencies do not commute, the eigenvalue density of the broadband matrix A will be very different.

First, we study the simpler situation when A is given by a sum of matrices at discrete frequencies that we assume are so widely separated that correlations between them are negligible. Hence initially we take $I(\omega) = \sum_{m=1}^{M} W_m \delta(\omega - \omega_m)$ and assume no correlation between the M matrices, $\{t(\omega_m) \equiv t_m\}$. The setup for $M = 2$ is illustrated in Fig. 1(a). The eigenvalue density for a sum of large, mutually uncorrelated, non-commuting random matrices can be treated by methods developed in free probability theory, which generalizes the concept of statistical independence to such matrices [36, 37]. Specifically one can apply an addition rule [38] to find an implicit equation for the eigenvalue density of their sum. For the matrix A, define $g_A(z)$ as the Stieltjes transform (resolvent) of the eigenvalue density p_A; applying the addition rule, one finds that the unknown resolvent g_A can be obtained from the following implicit equation (details in [39])

$$z + \frac{M-1}{g_A(z)} = \sum_{m=1}^{M} W_m g^{-1}_{t_m^\dagger t_m}(W_m g_A(z)), \qquad (2)$$

with the known resolvent $g_{t_m^\dagger t_m}$ that is determined from the bimodal distribution $p_{t_m^\dagger t_m}$. We then apply standard root-finding algorithms to this equation to find $g_A(z)$ and obtain the desired eigenvalue density through the inverse Stieltjes transform $p_A(T) = -\lim_{\epsilon\to 0^+} \mathrm{Im} g_A(T + i\epsilon)/\pi$. Results for the general ($M > 2$) cases are given in Fig. S1 in [39]. Here we examine the simpler $M = 2$ case for different combinations of weights $\{W_1, W_2\}$, shown as solid curves in Fig. 1(b) (here, $\bar{T}_1 = 0.027$, $\bar{T}_2 = 0.021$). The $W_1 = 0$, $W_2 = 1$ case corresponds to the monochromatic bimodal distribution. With increasing W_1, the upper edge $T_{\max}$ decreases as expected; the residual peaks near $T \approx W_1$ and $T \approx W_2$ can be traced back to the open channels of the constituent matrices $W_1 t_1^\dagger t_1$ and $W_2 t_2^\dagger t_2$. From the case $W_1 = W_2 = 1/2$, we see that $T_{\max} \approx 0.59$ is larger than the $(1 + \bar{T})/2 \approx 1/2$ one would obtain from using the monochromatic open channels as the input wavefront.

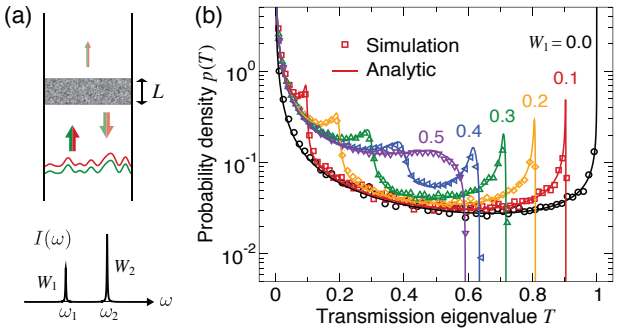

FIG. 1: Total transmission through a disordered slab for incident light with two discrete frequencies. (a) Schematic setup, with a disordered slab in a multimode waveguide and polychromatic light incident with a shared wavefront. (b) Density of the polychromatic transmission eigenvalues as calculated numerically by solving the wave equation (symbols) and analytically using Eq. (2) from free probability theory (lines). Numbers indicate the intensity weight W_1.

We perform numerical simulations to validate the analytic prediction. As illustrated in Fig. 1(a), we simulate a 2D disordered slab of thickness L and width $W = 3L$ in a waveguide geometry with background refractive index $n_0 = 1.5$ and slab permittivity $\epsilon(\mathbf{r})$ randomly sampled between $n_0^2 \pm 0.9$ at each grid point. Using the recursive Green's function method [48], we obtain the N-by-N transmission matrix (here $N = 647$) of the wave equation $[\nabla^2 + (\omega/c)^2\epsilon(\mathbf{r})]\psi(\mathbf{r}) = 0$ for 600 realizations of disorder, at two frequencies $\omega_1 = 390c/L$ and $\omega_2 = 410c/L$ (average transmissions $\bar{T}_1 = 0.027$, $\bar{T}_2 = 0.021$; the variation of N is negligible) that are much further than $\delta\omega$ apart (here $\omega_2 - \omega_1 \approx 290\delta\omega$). The resulting eigenvalue densities of the two-frequency matrix A, shown as symbols in Fig. 1(b), agree perfectly with the analytic prediction with no fitting parameters.

To see the effect of spectral correlations, we perform simulations for a broadband input with uniform spectral weights $I(\omega)$ over bandwidth $\Delta\omega$, centered at $\omega_0 = 400c/L$ (where $\bar{T} = 0.025$). The numerically obtained maximum eigenvalue $T_{\max}$ of the broadband matrix A is plotted as blue circles in Fig. 2(a), as a function of $\Delta\omega/\delta\omega$, where $\delta\omega = 0.069c/L \approx 21D/L^2$ is defined as the full width at half maximum (FWHM) of the transmission spectrum for the monochromatic open channel (black line in Fig. 2(b)); note that the FWHM of the open channel transmission coincides with the FWHM of the speckle intensity correlation (see Fig. S2 in [39]). In Fig. 2(a), we find that at all bandwidths, $T_{\max}$ (blue circles) is much larger than the prediction of the uncorrelated model when the effective number of independent frequencies is taken as $M_{\text{eff}} = 1 + \Delta\omega/\delta\omega$ (green dashed line), which itself is larger than the frequency-averaged transmission of the monochromatic open chan-

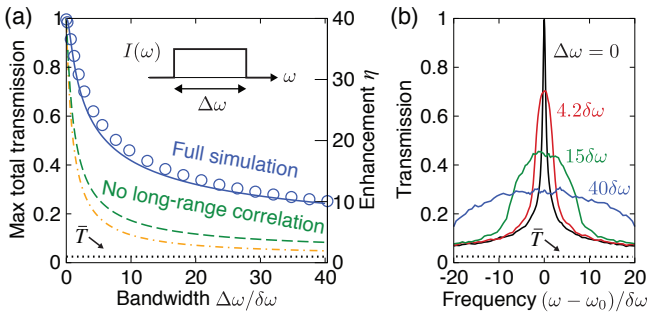

FIG. 2: Broadband transmission open channels. (a) Maximal eigenvalue $T_{\max}$ of the broadband flux matrix A and the enhancement $\eta = T_{\max}/\bar{T}$ obtained from numerical simulations (blue circles) and analytic theory accounting for long-range correlation (blue line), showing the highest achievable frequency-integrated transmission across bandwidth $\Delta\omega$. The two lines below show the would-be maximal transmission (green, dashed) and the transmission of the monochromatic open channel (orange, dot-dashed) if there were $1 + \Delta\omega/\delta\omega$ uncorrelated frequencies. Black dotted line indicates the average transmission. (b) Transmission as a function of frequency when the input wavefront is fixed to the optimal eigenvector with different bandwidths $\Delta\omega$.

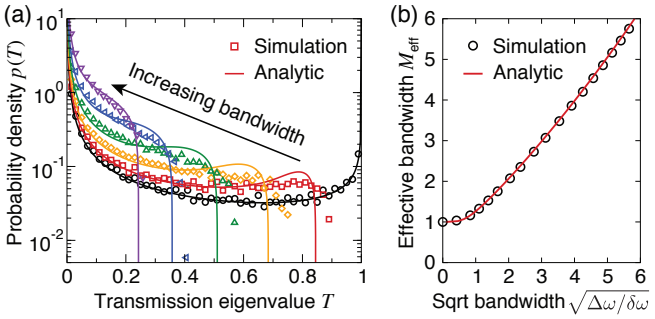

FIG. 3: (a) Density of the broadband transmission eigenvalues for various bandwidths, calculated numerically from simulations (symbols; bandwidths $\Delta\omega/\delta\omega = 0,\ 1.0,\ 2.4,\ 5.9,\ 15,\ 40$) and analytically from Eq. (3) with an effective number M_{eff} of independent frequencies (lines; $M_{\text{eff}} = 1.0, 1.3, 1.7, 2.4, 3.9, 6.6$). (b) M_{eff} as a function of the square-root bandwidth, evaluated numerically from Eq. (4) (symbols) and analytically from Eqs. (5)-(6) (line).

nel, $(1 + \bar{T}\Delta\omega/\delta\omega)/(1 + \Delta\omega/\delta\omega)$, when one assumes $M_{\text{eff}} = 1 + \Delta\omega/\delta\omega$ (orange dot-dashed line). The transmission spectra of the optimal broadband eigenvectors cover the target bandwidth rather uniformly, as shown in Fig. 2(b) for representative bandwidths.

To account for the spectral correlations, we adopt an approach similar to the treatment of spatial correlations in Ref. [6]. We hypothesize that even in the presence of spectral correlations, the eigenvalue density can still be described by Eq. (2), but with M replaced by some effective number of independent frequencies, $M_{\text{eff}} < 1 + \Delta\omega/\delta\omega$. We focus on the case where the spectral weights W_m is uniform, for which Eq. (2) takes a simpler form

$$\frac{g_A(z)}{M_{\text{eff}}} = g_{t^\dagger t}\left(z + \frac{M_{\text{eff}} - 1}{g_A(z)}\right). \tag{3}$$

This coincides with Eq. (3) in Ref. [14] when A is taken to be $\tilde{t}^\dagger\tilde{t}$ with $\tilde{t}$ being a "filtered" matrix that only has a fraction $m_1 = 1/M_{\text{eff}}$ of the input channels (columns) of the full matrix t, as in experiments where all output lights are measured but only a fraction of the incident channels is controlled by the SLM [6]. Given this equivalence, we can use a property of the filtered matrix [14]

$$\frac{1}{M_{\text{eff}}} = \frac{\text{Var}(\tilde{\tau})}{\text{Var}(\tau)}, \tag{4}$$

to determine M_{eff}, where $\tilde{\tau}$ and τ are the eigenvalues of A and of $t_m^\dagger t_m$ respectively. With the broadband eigenvalue density from simulations (symbols in Fig. 3(a)), we confirm that Eq. (4) provides the correct value of M_{eff} that, through Eq. (3), predicts analytical eigenvalue densities (lines in Fig. 3(a)) that agree well with the numerical data. M_{eff} obtained in this manner scales with the square root of the bandwidth (circles in Fig. 3(b)).

The quantity $\text{Var}(\tilde{\tau})$ can be expressed in terms of the disorder average of certain products of four transmission amplitudes t_{ab}, and the disorder averages can be carried out analytically using impurity-averaged perturbation theory (details in [39] and Figs. S3-S4). We find

$$\frac{1}{M_{\text{eff}}} = \iint \frac{d\omega_1 d\omega_2}{\Delta\omega^2} \frac{C^{(T)}(\omega_1, \omega_2)}{C^{(T)}(\omega_0, \omega_0)}, \tag{5}$$

where $C^{(T)}(\omega_1, \omega_2)$ is the mean-normalized spectral correlation $\langle T_a(\omega_1)T_a(\omega_2)\rangle/\langle T_a(\omega_1)\rangle\langle T_a(\omega_2)\rangle - 1$ of the total transmission $T_a = \sum_b |t_{ba}|^2$, with the brackets denoting average over disordered samples; the dependence on mode index a drops out due to the normalization. In our system, $C^{(T)}$ is well described by (see Fig. S4(a) in [39])

$$C^{(T)}(\omega_1, \omega_2) = \frac{1}{N\bar{T}}\left[\frac{2}{x}\frac{\sinh(x) - \sin(x)}{\cosh(x) - \cos(x)} - \bar{T}\right], \tag{6}$$

where $x = \sqrt{2|\omega_1 - \omega_2|L^2/D}$. In Eq. (6), the first term is the long-range correlation that decays as $|\omega_1 - \omega_2|^{-1/2}$ (see Ref. [23]), while the second term is a finite-$\bar{T}$ correction [39, 49]. Eqs. (5)-(6) provide an analytic expression to calculate M_{eff} without free parameters and perfectly agrees with the M_{eff} obtained from simulations, as shown in Fig. 3(b). The blue solid line in Fig. 2(a) is calculated with this analytic expression of M_{eff}, and it explains the much larger potential transmission enhancement through WFS than expected from the uncorrelated model. Specifically, when $\Delta\omega$ falls in the regime $1 \ll \sqrt{\Delta\omega/\delta\omega} \ll 1/\bar{T}$, the relevant values of $C^{(T)}$ are dominated by the $|\omega_1 - \omega_2|^{-1/2}$ tail in the long-range contribution, giving rise to the scaling of $M_{\text{eff}} \approx \sqrt{\Delta\omega/\delta\omega}$ and a larger $T_{\max}$. Note that Eqs. (5)-(6) show that M_{eff} and $T_{\max}$ depend only on $\Delta\omega$ and $\bar{T}$.

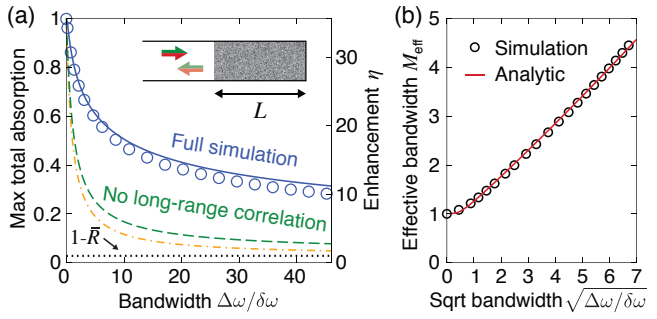

FIG. 4: Broadband coherently enhanced absorption (CEA). (a) Maximal frequency-integrated absorption $1-R_{\min}$ and the enhancement $\eta = (1-R_{\min})/(1-\bar{R})$ obtained numerically (blue circles) and analytically (blue line) across bandwidth $\Delta\omega$. The two lines below show the would-be maximal absorption (green, dashed) and the absorption of the monochromatic CEA mode (orange, dot-dashed) if there were $1+\Delta\omega/\delta\omega$ uncorrelated frequencies. Black dotted line indicates the average absorption. Inset shows schematic setup of the system; a reflecting boundary on the right ensures that transmission is zero and absorption is $1-R$. (b) M_{eff} as a function of the square-root bandwidth, evaluated numerically from Eq. (4) (symbols) and analytically from Eqs. (5) and (7) (line).

The presence of weak absorption modifies the long-range spectral correlation in transmission but does not change the $|\omega_1-\omega_2|^{-1/2}$ scaling [50, 51], so the above-mentioned effects persist. In fact, in absorbing systems, long-range correlations in reflection [24] can help the broadband operation of coherently enhanced absorption (CEA). Consider a thick diffusive scattering medium with $\lambda \ll l \ll \sqrt{ll_a/d} < L$, where l_a is the ballistic absorption length. As the thickness L is larger than the diffusive absorption length $L_a = \sqrt{ll_a/d}$, the transmitted flux is exponentially small, so any light that is not reflected can be considered absorbed. As $l \ll l_a$, most incident light is reflected before it propagates far enough to be absorbed, so the average absorption is low. However, there exist eigenchannels that can be nearly completely absorbed at one frequency when the number of input channels (*i.e.* degrees of freedom to be controlled) is large enough that $N^2 l/l_a \gg 1$ [12, 52]. The minimum reflection (corresponding to the maximum absorption) is the smallest eigenvalue of $r^\dagger r$, and in the $N\to\infty$ limit the monochromatic eigenvalues follow a known bimodal distribution, $p_{r^\dagger r}(R) = 2a\sqrt{(1-R)/(aR)-1}/(\pi(1-R)^2)$, where $a \equiv l/l_a \ll 1$ [53, 54]. For broadband light with spectrum $I(\omega)$, we instead look for the eigenvalues of A as defined in Eq. (1) just with $t(\omega)$ replaced by $r(\omega)$.

We perform numerical simulations for the geometry shown in the inset of Fig. 4(a) with thickness L and width $W = 0.43L$ and with a weak uniform absorption $\text{Im}(\epsilon) = 3\times10^{-5}$ in the diffusive medium (corresponding to $a = 2\times10^{-4}$, $\bar{R} = 0.97$, and $N = 323$ near $\omega_0 = 1400c/L$). Again, we consider broadband incident light with uniform spectral weights $I(\omega)$ over bandwidth $\Delta\omega$, and numerically evaluate the reflection matrices $r(\omega)$ and the eigenvalues of the broadband flux matrix A. The maximum absorption, $1-R_{\min}$, is plotted as blue circles in Fig. 4(a) as a function of $\Delta\omega/\delta\omega$, where $\delta\omega = 0.14c/L \approx 12c/l_a$ is defined as the FWHM of the absorption spectrum for the monochromatic CEA channel (see Fig. S5(a) in [39]). Similar to the broadband lossless transmission, here we find the maximal absorption to be much larger than the prediction if one were to ignore long-range spectral correlations (green dashed and orange dot-dashed lines).

The density of broadband reflection eigenvalues is well described by Eq. (3) with $t^\dagger t$ replaced by $r^\dagger r$ and with M_{eff} given by Eq. (4) (see Fig. S5(b) in [39]), confirming the hypothesis that one can use an effective number of independent frequencies to describe the broadband eigenvalue distribution. Analytically, M_{eff} is again given by Eq. (5), just with $C^{(T)}$ replaced by the spectral correlation $C^{(R)}(\omega_1,\omega_2) \equiv \langle R_a(\omega_1)R_a(\omega_2)\rangle/\langle R_a(\omega_1)\rangle\langle R_a(\omega_2)\rangle - 1$ of the total reflection $R_a = \sum_b |r_{ba}|^2$, which in our system is well described by (see Fig. S4(b) in [39])

$$C^{(R)}(\omega_1,\omega_2) = \frac{1-\bar{R}}{N\bar{R}(1+\bar{R})}\left[\frac{2}{1+y} - (1-\bar{R})\right], \quad (7)$$

where $y = \text{Re}\sqrt{1+i|\omega_1-\omega_2|l_a/c}$. Here, the first term decays as $|\omega_1-\omega_2|^{-1/2}$ and is the long-range reflection correlation derived in Ref. [24], while the second term is a correction for finite $1-\bar{R}$ [39]. Eqs. (5) and (7) provide an analytic expression for M_{eff} and is plotted as the red line in Fig. 4(b), with its prediction of the maximal absorption plotted as the blue line in Fig 4(a). When the bandwidth $\Delta\omega$ falls in the regime $1 \ll \sqrt{\Delta\omega/\delta\omega} \ll 1/(1-\bar{R})$, the $C^{(R)}$ is dominated by the $|\omega_1-\omega_2|^{-1/2}$ tail in the long-range contribution, and M_{eff} scales as $\sqrt{\Delta\omega/\delta\omega}$.

Although using a single spatial wavefront to control broadband light introduces a loss of control, we have shown that long-range spectral correlations of the total transmission and reflection in the diffusive regime [55] significantly reduce this loss, making strong enhancements possible across bandwidths $\Delta\omega$ much larger than the spectral correlation width $\delta\omega$ of the medium. Spatial WFS is typically realized in optics, but this effect also applies to the diffusive transport of electrons and acoustic waves. The incomplete spatial control of the input due to limited numerical aperture or finite illumination area on a wide slab can be incorporated in our formalism by replacing t and r with the filtered matrices $\tilde{t}$ and $\tilde{r}$ [6, 14]; see [39] for details. The results for uncorrelated matrices (Eq. (2)) can also treat spatially incoherent light with multiple uncorrelated transverse modes or unpolarized light with two independent polarizations. Furthermore, the eigenproblem formalism in the present work can be extended to study the total transmitted flux at a given time of flight [39].

We acknowledge helpful discussions with Seng Fatt Liew, Alexey Yamilov, Raktim Sarma, and Steven G Johnson. This work is supported by the National Science Foundation under grant No. DMR-1307632, DMR-1205307, and ECCS-1068642, and by the US Office of Naval Research under grant No. N00014-13-1-0649. A.G. acknowledges the support of LABEX WIFI (Laboratory of Excellence ANR-10-LABX-24) within the French Program "Investments for the Future" under reference ANR-10-IDEX-0001-02 PSL*.

* Electronic address: chiawei.hsu@yale.edu

[1] A. P. Mosk, A. Lagendijk, G. Lerosey, and M. Fink, Nature Photon. **6**, 283 (2012).
[2] R. Horstmeyer, H. Ruan, and C. Yang, Nature Photon. **9**, 563 (2015).
[3] I. M. Vellekoop and A. P. Mosk, Opt. Lett. **32**, 2309 (2007).
[4] I. M. Vellekoop and A. P. Mosk, Phys. Rev. Lett. **101**, 120601 (2008).
[5] M. Kim, Y. Choi, C. Yoon, W. Choi, J. Kim, Q.-H. Park, and W. Choi, Nature Photon. **6**, 581 (2012).
[6] S. M. Popoff, A. Goetschy, S. F. Liew, A. D. Stone, and H. Cao, Phys. Rev. Lett. **112**, 133903 (2014).
[7] B. Gérardin, J. Laurent, A. Derode, C. Prada, and A. Aubry, Phys. Rev. Lett. **113**, 173901 (2014).
[8] O. N. Dorokhov, Solid State Commun. **51**, 381 (1984).
[9] Y. Imry, Europhys. Lett. **1**, 249 (1986).
[10] P. A. Mello, P. Pereyra, and N. Kumar, Ann. Phys. **181**, 290 (1988).
[11] Y. V. Nazarov, Phys. Rev. Lett. **73**, 134 (1994).
[12] Y. D. Chong and A. D. Stone, Phys. Rev. Lett. **107**, 163901 (2011).
[13] S. F. Liew, S. M. Popoff, S. W. Sheehan, A. Goetschy, C. A. Schmuttenmaer, A. D. Stone, and H. Cao (2015), arXiv:1507.07438.
[14] A. Goetschy and A. D. Stone, Phys. Rev. Lett. **111**, 063901 (2013).
[15] H. Yu, T. R. Hillman, W. Choi, J. O. Lee, M. S. Feld, R. R. Dasari, and Y. K. Park, Phys. Rev. Lett. **111**, 153902 (2013).
[16] E. Akkermans and G. Montambaux, *Mesoscopic Physics of Electrons and Photons* (Cambridge University Press, Cambridge, UK, 2007).
[17] F. van Beijnum, E. G. van Putten, A. Lagendijk, and A. P. Mosk, Opt. Lett. **36**, 373 (2011).
[18] E. Small, O. Katz, Y. Guan, and Y. Silberberg, Opt. Lett. **37**, 3429 (2012).
[19] H. P. Paudel, C. Stockbridge, J. Mertz, and T. Bifano, Opt. Express **21**, 17299 (2013).
[20] D. Andreoli, G. Volpe, S. Popoff, O. Katz, S. Grésillon, and S. Gigan, Sci. Rep. **5**, 10347 (2015).
[21] M. J. Stephen and G. Cwilich, Phys. Rev. Lett. **59**, 285 (1987).
[22] S. Feng, C. Kane, P. A. Lee, and A. D. Stone, Phys. Rev. Lett. **61**, 834 (1988).
[23] R. Pnini and B. Shapiro, Phys. Rev. B **39**, 6986 (1989).
[24] D. B. Rogozkin and M. Y. Cherkasov, Phys. Rev. B **51**, 12256 (1995).
[25] P. A. Mello, E. Akkermans, and B. Shapiro, Phys. Rev. Lett. **61**, 459 (1988).
[26] R. Berkovits and S. Feng, Phys. Rep. **238**, 135 (1994).
[27] R. Pnini, in *Waves and Imaging through Complex Media*, edited by P. Sebbah (Springer, Netherlands, 2001), pp. 391–412.
[28] P. Sheng, *Introduction to Wave Scattering, Localization and Mesoscopic Phenomena* (Springer-Verlag, Berlin, 2006), 2nd ed.
[29] W. Choi, A. P. Mosk, Q.-H. Park, and W. Choi, Phys. Rev. B **83**, 134207 (2011).
[30] Z. Shi and A. Z. Genack, Phys. Rev. Lett. **108**, 043901 (2012).
[31] S. F. Liew, S. M. Popoff, A. P. Mosk, W. L. Vos, and H. Cao, Phys. Rev. B **89**, 224202 (2014).
[32] A. Peña, A. Girschik, F. Libisch, S. Rotter, and A. A. Chabanov, Nat Commun **5**, 3488 (2014).
[33] M. Davy, Z. Shi, J. Wang, X. Cheng, and A. Z. Genack, Phys. Rev. Lett. **114**, 033901 (2015).
[34] M. Davy, Z. Shi, J. Park, C. Tian, and A. Z. Genack, Nat. Commun. **6**, 6893 (2015).
[35] P. W. Brouwer, Phys. Rev. B **57**, 10526 (1998).
[36] D. V. Voiculescu, K. J. Dykema, and A. Nica, *Free random variables* (American Mathematical Society, Providence, RI, USA, 1992).
[37] A. M. Tulino and S. Verdú, *Random Matrix Theory and Wireless Communications* (Now Publishers, Delft, Netherlands, 2004).
[38] D. Voiculescu, J. Funct. Anal. **66**, 323 (1986).
[39] See Supplementary Material, which includes Refs. [40-47], for the derivations of Eqs. (2) and (5), results of the uncorrelated model when $M > 2$, incorporation of incomplete spatial channel control, spectral correlation data for the monochromatic open channel and CEA channel, reflection eigenvalue distributions, finite-$\bar{T}$ and finite $1 - \bar{R}$ corrections of the transmission and reflection correlations, and extension to total transmission at a given time of flight.
[40] P. A. Mello and A. D. Stone, Phys. Rev. B **44**, 3559 (1991).
[41] L. Wang and S. Feng, Phys. Rev. B **40**, 8284 (1989).
[42] R. Berkovits, Phys. Rev. B **42**, 10750 (1990).
[43] P. A. Lee and A. D. Stone, Phys. Rev. Lett. **55**, 1622 (1985).
[44] P. A. Mello, J. Phys. A **23**, 4061 (1990).
[45] J. F. de Boer, M. P. van Albada, and A. Lagendijk, Phys. Rev. B **45**, 658 (1992).
[46] A. A. Lisyansky and D. Livdan, Phys. Rev. B **47**, 14157 (1993).
[47] M. van Rossum and T. Nieuwenhuizen, Phys. Lett. A **177**, 452 (1993).
[48] H. U. Baranger, D. P. DiVincenzo, R. A. Jalabert, and A. D. Stone, Phys. Rev. B **44**, 10637 (1991).
[49] A. García-Martín, F. Scheffold, M. Nieto-Vesperinas, and J. J. Sáenz, Phys. Rev. Lett. **88**, 143901 (2002).
[50] R. Pnini and B. Shapiro, Phys. Lett. A **157**, 265 (1991).
[51] E. Kogan and M. Kaveh, Phys. Rev. B **45**, 1049 (1992).
[52] One can interpret the $N^2 l/l_a \gg 1$ condition heuristically: strong absorption requires penetration depth of L_a, and in a low-loss medium, existence of high-transmission channels into depth L_a requires $g = Nl/L_a \gg 1$.
[53] N. A. Bruce and J. T. Chalker, J. Phys. A **29**, 3761 (1996).
[54] C. W. J. Beenakker, J. C. J. Paasschens, and P. W.

Brouwer, Phys. Rev. Lett. **76**, 1368 (1996).
[55] In the localization regime, the mode linewidths are narrower than the mean level spacing, and transmission proceeds through a single mode; in such case, the optimal broadband wavefront and its transmission are those of that single mode unless the bandwidth $\Delta\omega$ is larger than mode spacing.